Aerodynamic Characteristics of Noncircular Bodies in Flat Spin and Coning Motions

L. E. Ericsson*
Lockheed Missiles & Space Company, Inc., Sunnyvale, California

Experimental results for bodies of square cross-section coning at angles up to 90 deg show that the measured side force characteristics are extremely nonlinear, exhibiting both discontinuities and hysteresis effects. The present paper analyzes these results to determine to what extent the nonsteady wall boundary condition has influenced the flow separation and associated lateral characteristics of the coning body. It is shown that the so-called moving wall effects have a dominant influence on the flow separation and can explain the unusual side force characteristics measured in the experiments.

Nomenclature

c = cross-sectional chord (diameter for a circular cross section)
h = cross-sectional maximum height
L^l = sectional lift; coefficient, $c_l = L^l/(\rho_\infty U_\infty^2/2)c$
M = freestream Mach number
N = coning rate
N^l = sectional normal force coefficient, $c_n = N^l/(\rho_\infty U_\infty^2/2)c$
p = roll rate
P = static pressure; coefficient, $C_p = (p-p_\infty)/(\rho_\infty U_\infty^2/2)$
r = corner radius
Re = Reynolds number, $= U_\infty c/\nu_\infty$
U = velocity
x = distance forward of coning axis (Fig. 1)
Y = side force; coefficient, $C_y = y/(\rho_\infty U_\infty^2/2)(\pi c^2/4)$
α = angle of attack
ν = kinematic viscosity of air
ξ = dimensionless x coordinate, $= x/c$
ρ = air density
σ = angle between freestream velocity vector and body axis
ψ = local sideslip angle, $\approx U_w/U_\infty = (\xi\Omega/3)\sin\sigma$
ω = angular spin rate
Ω = reduced spin rate, $= 3\omega c/U_\infty$ (In Ref. 1, $\Omega = \omega b/2U_\infty$, where b is the wing span, $= 6c$.)

Subscripts

w = wall
∞ = freestream conditions

Introduction

EXPERIMENTAL results have been obtained at coning angles of up to 90 deg for bodies of square cross section using a rotary balance[1-3] (Fig. 1). The measured side force characteristics at subcritical, critical, and supercritical Reynolds numbers are highly nonlinear, exhibiting discontinuities and hysteresis effects. It is shown herein how these results can be explained when considering the nonsteady wall boundary condition, the so-called moving wall effect.[4-6]

Presented as Paper 84-0508 at the AIAA 22nd Aerospace Sciences Meeting, Reno, Nev., Jan. 9-12, 1984; received Feb. 6, 1984; revision received Oct. 4, 1984.

*Senior Consulting Engineer. Fellow AIAA.

Data Analysis

Flat spin results for a body with a square cross section display highly nonlinear lateral aerodynamic characteristics[1] (Fig. 2) (note that ψ_{max} is the maximum local flow inclination existing at the nose tip). The measured side force of the forebody (forward of the rotation center) reaches high values. $|C_y| > 2$, when the motion-induced sideslip angle at the nose is only a few degrees. And not until high supercritical and transcritical Reynolds numbers (this reclassification is the one used by Achenbach[7]) does the side force take the linear, stabilizing $C_y(\Omega)$ shape expected for attached flow (forward of the cross-sectional base). At lower Reynolds numbers, destabilizing, highly nonlinear $C_y(\Omega)$ characteristics are measured, exhibiting discontinuities and hysteresis effects of various kinds. In what follows, the flow phenomena responsible for this multitude of nonlinear aerodynamic behaviors will be discussed.

Whereas at lower angles of attack, $\alpha < 60$ deg, the steady symmetric and asymmetric vortices generated by the forebody[8] would play a significant part in the vehicle dynamics,[5,9] at $\alpha > 60$ deg the vortices become of the unsteady von Kármán type[5,10] and cannot couple with the body motion in any general sense. The two-dimensional coupling described in Refs. 4 and 6 for a cylinder describing translatory oscillations in cross flow cannot be realized for a body in flat spin motion. Instead the situation is analogous to that for a rotating cylinder,[11] in which case it is found[6] that the moving wall effect on the asymmetric flow separation is unaffected by the Kármán vortex shedding.

Another concern is the effects of centrifugal and Coriolis forces on the chordwise flow, especially with regard to the flow separation.[11] A similar flowfield exists on a helicopter rotor blade. Tarzanin found that the blade stall did not start at the tip and spread gradually inward on the retreating blade as the stall angle was exceeded locally. Instead, stall started simultaneously over the outboard 40% of the blade span. Apparently, the blade rotation in the chordwise plane caused this spanwise correlation of the dynamic stall process. Consequently, one would expect the square cross-sectional forebody in Fig. 1 to have its unsteady flow separation correlated over the first 40%. Thus, the aerodynamic characteristics in Fig. 2 are determined to a large extent, by the effect of local cross flow and moving wall velocity on the flow separation in the near-nose region.

Subcritical Flow Conditions

In Fig. 3 the results at $M = 0.10$ for $Re = 0.15 \times 10^6$ (Fig. 2a) are shown together with sketches of suggested flow conditions. At $|\Omega| < 0.05$, or $|\psi_{max}| < 2$ deg, a destabilizing

(prospin) side force slope $dC_y/d\Omega$ is measured. This corresponds to a negative $c_{n\alpha}$ for the square cross section. Static experimental results for a rectangular cross section exhibit such negative $c_n(\alpha)$ and $c_l(\alpha)$ characteristics (Fig. 4). At angle of attack the curvature of the windward-side separated flow boundary is sharpened, increasing the suction, whereas the opposite occurs on the leeward side, resulting in the generation of a negative nose load[13] (Fig. 5).

The flow sketches in Fig. 6 illustrate the fluid mechanical phenomena present for the translating square cross section. Figure 6a shows the flow separation for stationary flow at zero flow inclination, $\alpha=\psi=0$. In Fig. 6b the effect of the translatory velocity $U_w=x\omega\sin\sigma$ on the flow separation is illustrated, and Fig. 6c shows the expected effect of a stationary flow inclination $\Psi=U_w/U_\infty=(\xi\Omega/3)\sin\sigma$. [The flow inclination angles are small ($\psi_{max}<2$ deg in Fig. 3) and arctan $U_w/U_\infty=U_w/U_\infty$.] The large difference between the $C_y(\psi)$ slope in Fig. 3 and the $c_l(\alpha)$ and corresponding $c_n(\alpha)$ slope in Fig. 4, which would be the expected $C_y(\psi)$ slope for stationary flow conditions, must be due to the unsteady boundary condition sketched in Fig. 6b, the so-called moving wall effect.[4,6] That downstream moving wall effect on the advancing side of the cross section delays the flow separation, as illustrated in Fig. 6b. Conversely, the upstream moving wall effect promotes separation on the retreating side. These downstream and upstream moving wall effects on flow separation are similar to the effects of increasing and decreasing Reynolds number, respectively. That the moving wall effects on viscous separated flow indeed can cause aerodynamic load changes very much larger than those for corresponding inviscid flow effects is demonstrated by the moving wall/leading-edge jet effect on dynamic stall, which causes a large overshoot of static lift maximum.[14-16]

The results in Fig. 4 are for a half-model of aspect ratio 5. The results shown in Fig. 7 were obtained for a two-dimensional model.[17] They show the same type of nonlinearity as the subcritical $C_y(\Omega)$ data in Fig. 2b for $M_\infty=0.25$. Figure 8 shows the results for $Re=0.15\times10^6$ together with sketches of suggested flow conditions. Apparently, increasing the Mach number from $M=0.10$ to 0.25 made the corner appear sharper to the flow, as would be expected from the usual compressibility effects. Thus, the $C_y(\Omega)$ slope is much milder (Fig. 7) than at $M=0.10$ (Fig. 3), and flow reattachment is established rather suddenly and not gradually.

In the static test, unsteady on-off reattachment might have given rise to the plateau in the time average $c_n(\alpha)$, appearing before the final c_n peak, as well as to the softness of the discontinuity. In contrast, the moving wall effects are unidirectional for the translating cross section, reinforcing the effect of ψ for $\Omega<\Omega_{crit}$ and causing a very rapid, almost jumpwise, change of C_y when Ω approaches Ω_{crit}, where $\Omega_{crit}\approx0.05$ in Fig. 8. This is in contrast to the gradual, continuous change of c_n when α approaches $\alpha_{crit}\approx12$ deg in Fig. 7.

When the critical value, α_{crit} or ψ_{crit}, is exceeded, the flow attaches on the windward side. In the static case, with $\alpha_{crit}\approx12$ deg, the leeward side contributes negligibly to $c_n(\alpha)$. In the dynamic case, however, where $\psi_{crit}<2$ deg, the leeward-side contribution is not negligibly small, and its negative lift generation, amplified by the moving wall effect, greatly

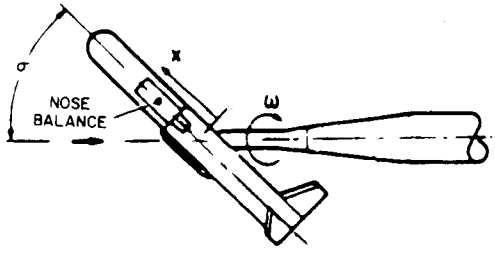

Fig. 1 Rotary balance and model.[1]

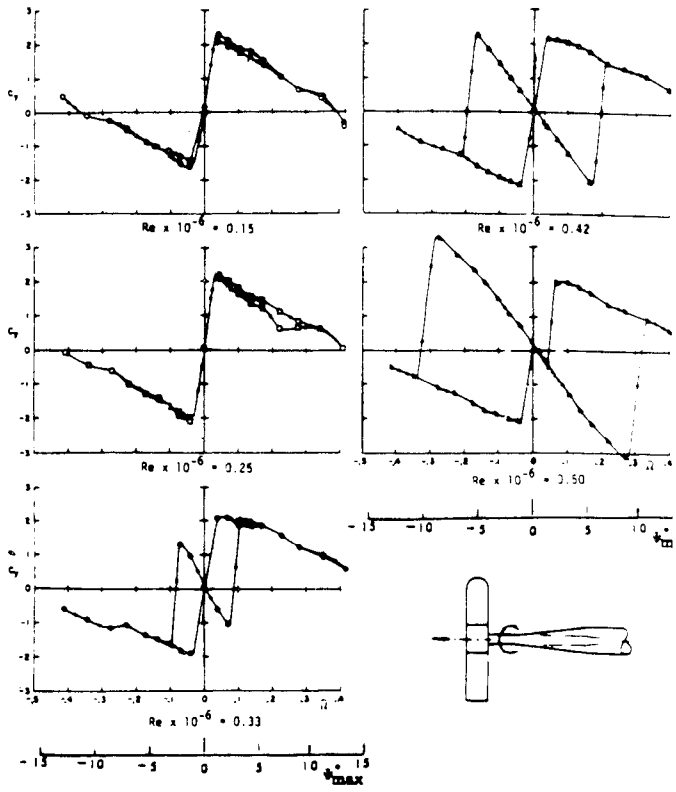

a) $M_\infty=0.10$.

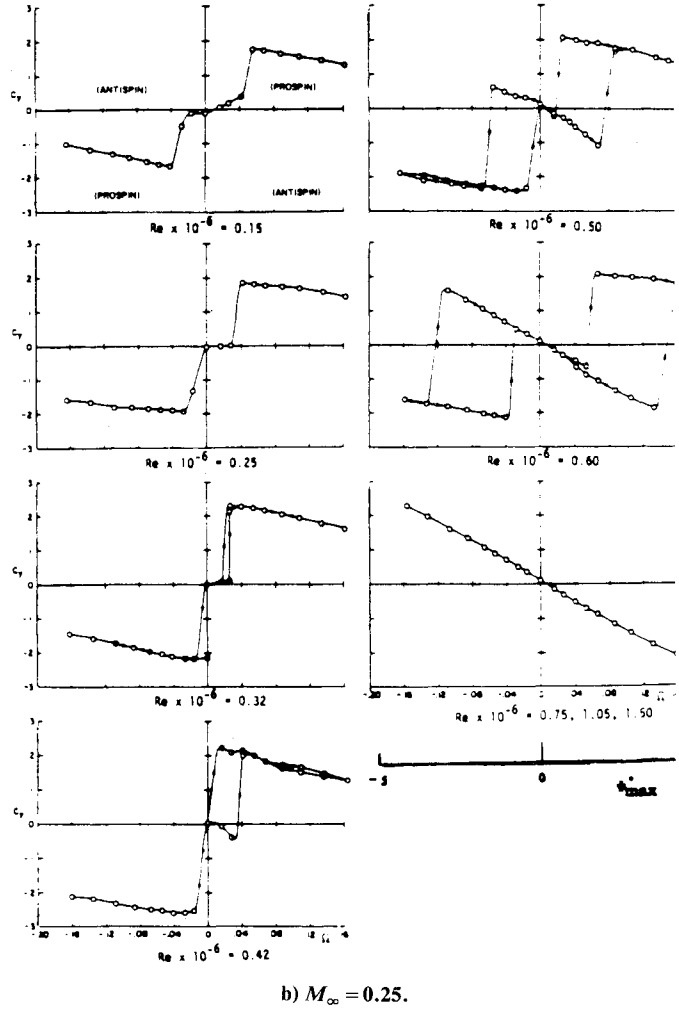

b) $M_\infty=0.25$.

Fig. 2 Forebody side force at $\alpha=90$ deg and varying M_∞ and Re.[1]

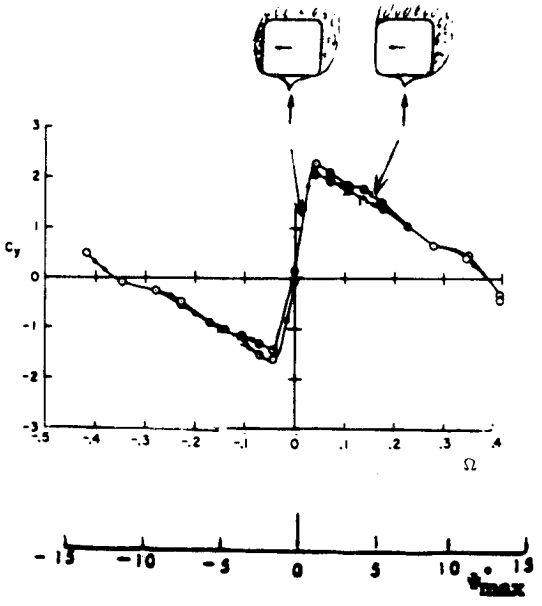

Fig. 3 Subcritical side force characteristics at $\sigma = 90$ deg, $M_\infty = 0.10$, and $Re = 0.15 \times 10^6$.

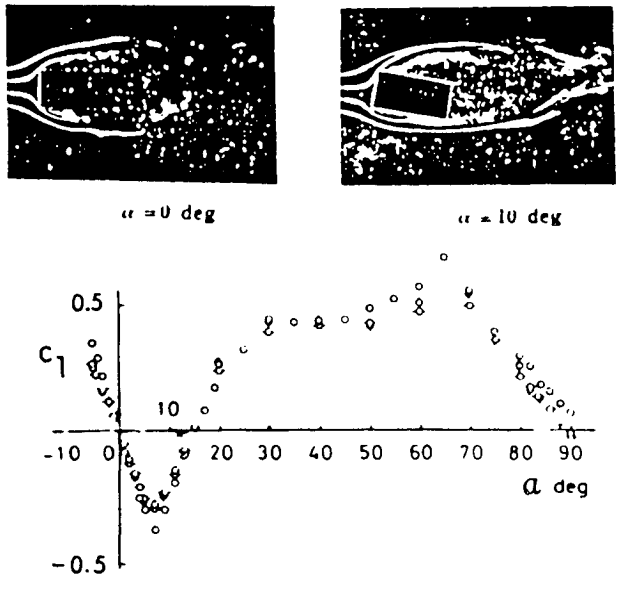

Fig. 4 Aerodynamic characteristics at low speeds of a rectangular prism.[12]

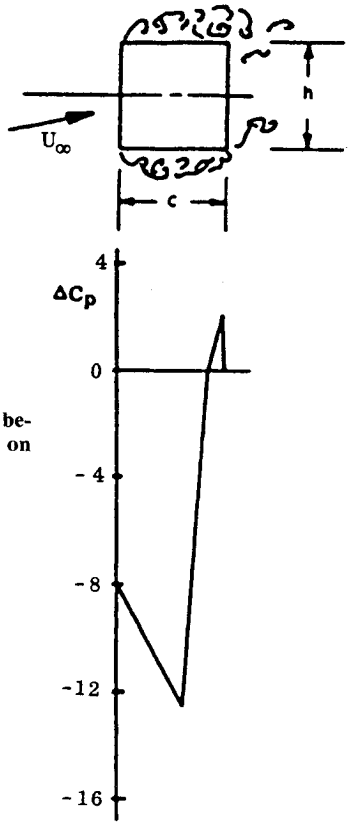

Fig. 5 Pressure differential between lower and upper surface on a square cross section.[13]

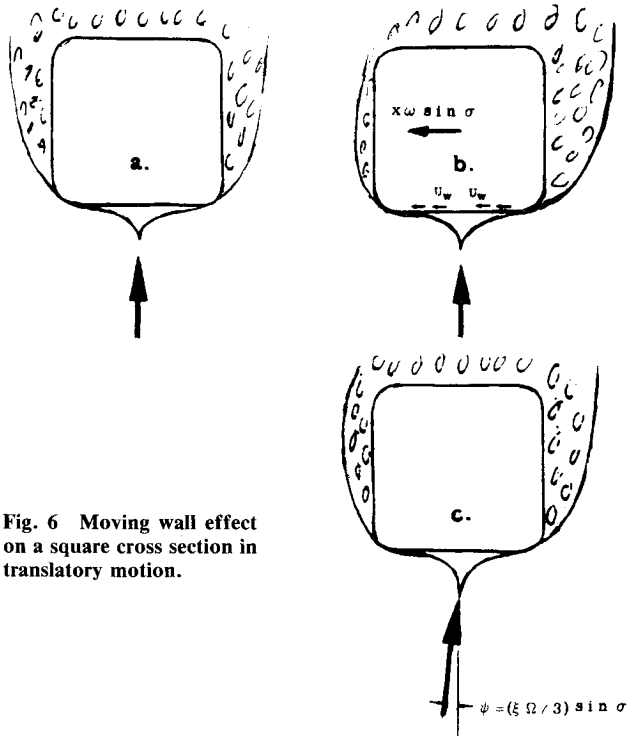

Fig. 6 Moving wall effect on a square cross section in translatory motion.

reduces the positive windward-side lift contribution. As a consequence, the negative $C_y(\Omega)$ slope for $\Omega > \Omega_{crit}$ is of considerably less magnitude than the positive $c_n(\alpha)$ slope for $\alpha > \alpha_{crit}$.

Of course, the cross sections in Figs. 3 and 8 have rounded corners, not sharp edges as those in Figs. 4 and 7. Experimental results show the corner radius to have a decisive effect on whether the subcritical total flow separation or the supercritical attached-flow behavior is obtained[18] (Fig. 9). The Reynolds number based upon corner radius appears to be the determining parameter (Fig. 10). The corner radius greatly enhances the moving wall effect, making it approach that for a circular cross section.[4-6]

Supercritical Flow Conditions

At higher Reynolds numbers, $Re \geq 0.33 \times 10^6$, the measured side force characteristics in Fig. 2 show that the flow is attached initially, at $\Omega = 0$. The reason is the same as for the supercritical static characteristics in Figs. 9 and 10, i.e., transition occurs on the front face of the cross section. In the static case, the flow remains attached up to a certain angle of attack, α_{crit}, which will vary slightly with Reynolds number. The tests by Polhamus[18] gave a value $\alpha_{crit} \approx 15$ deg for the large corner radius at $Re = 10^6$ (Fig. 11a). In the dynamic case, the upstream moving wall effect promotes transition to occur on the face and the associated supercritical attached-flow characteristics occur at a lower Reynolds number than in the static case (cf., Figs. 11a and 11b). Once the supercritical flow

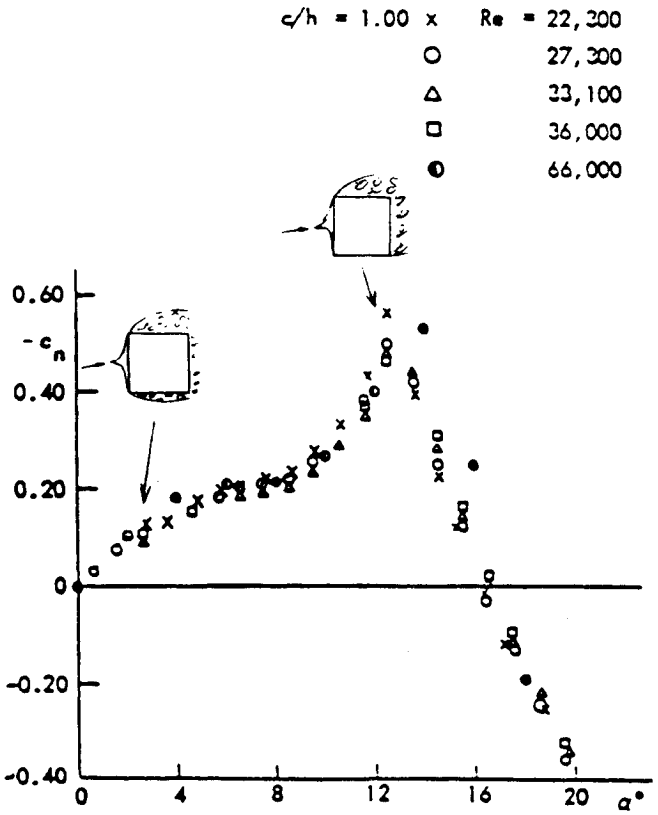

Fig. 7 Normal force characteristics of a sharp-edged square cross section.[17]

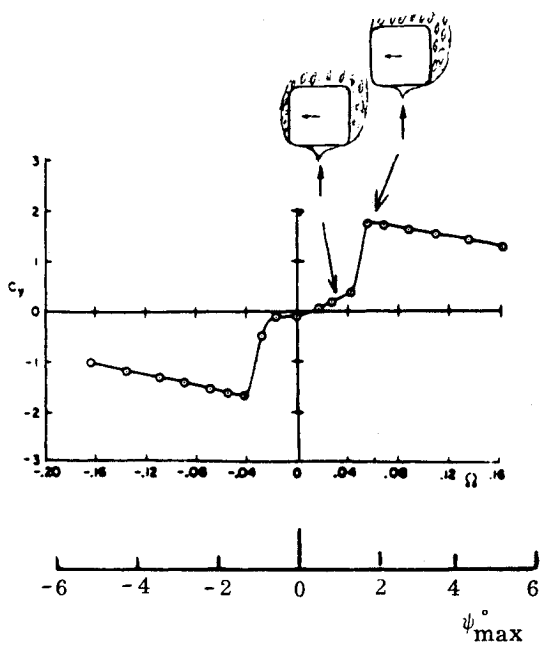

Fig. 8 Subcritical side force characteristics at $\sigma = 90$ deg, $M_\infty = 0.25$, and $Re = 0.15 \times 10^6$.

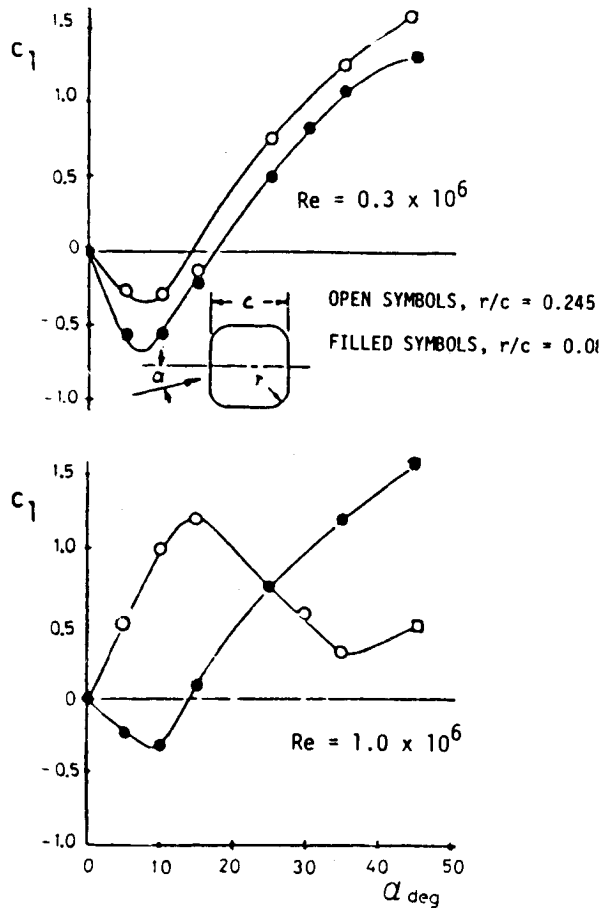

Fig. 9 Lift of a square cross section with rounded corners.[18]

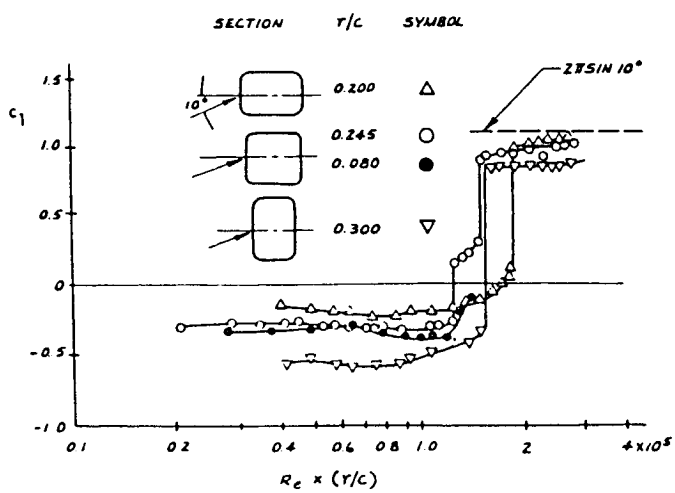

Fig. 10 Combined effect of corner radius and Reynolds number.[15]

is well established, the upstream moving wall effect will promote the flow separation occurring downstream of the transition point.[4-6] This causes the early separation shown in Fig. 11b for $Re = 0.33 \times 10^6$. As the Reynolds number is increased, the flow separation is delayed to higher ψ_{max} values, until $Re > 0.73 \times 10^6$ no separation occurred in the tested ψ range (Fig. 2). Considering the earlier discussed equivalence between the moving wall effect and the effect of Reynolds number, the measured Ω hysteresis (Figs. 2 and 11b) is in perfect agreement with the experimentally observed hysteresis for a circular cross section[19] (Fig. 12).

The static side force of the forebody measured by Malcolm and Clarkson[1] (Fig. 13) has the same sensitivity to Reynolds number as the two-dimensional normal force measured by Polhamus[18] (Figs. 9 and 10). A critical Reynolds number of 0.2×10^6, based upon the corner radius, is indicated ($r/c = 0.25$ in Fig. 13), which is in rather good agreement with the two dimensional results in Fig. 10 (Note that $C_y > 0$ corresponds to $c_n < 0$). Decreasing the angle of attack to $\sigma = 75$ deg lowers the critical Re somewhat, but the nonlinear behavior remains the same as for $\sigma = 90$ deg (Fig. 13). However, at $\sigma = 60$ and 45 deg, the characteristics become those typical of slender bodies with steady asymmetric vortices, in which case the side force becomes of largest

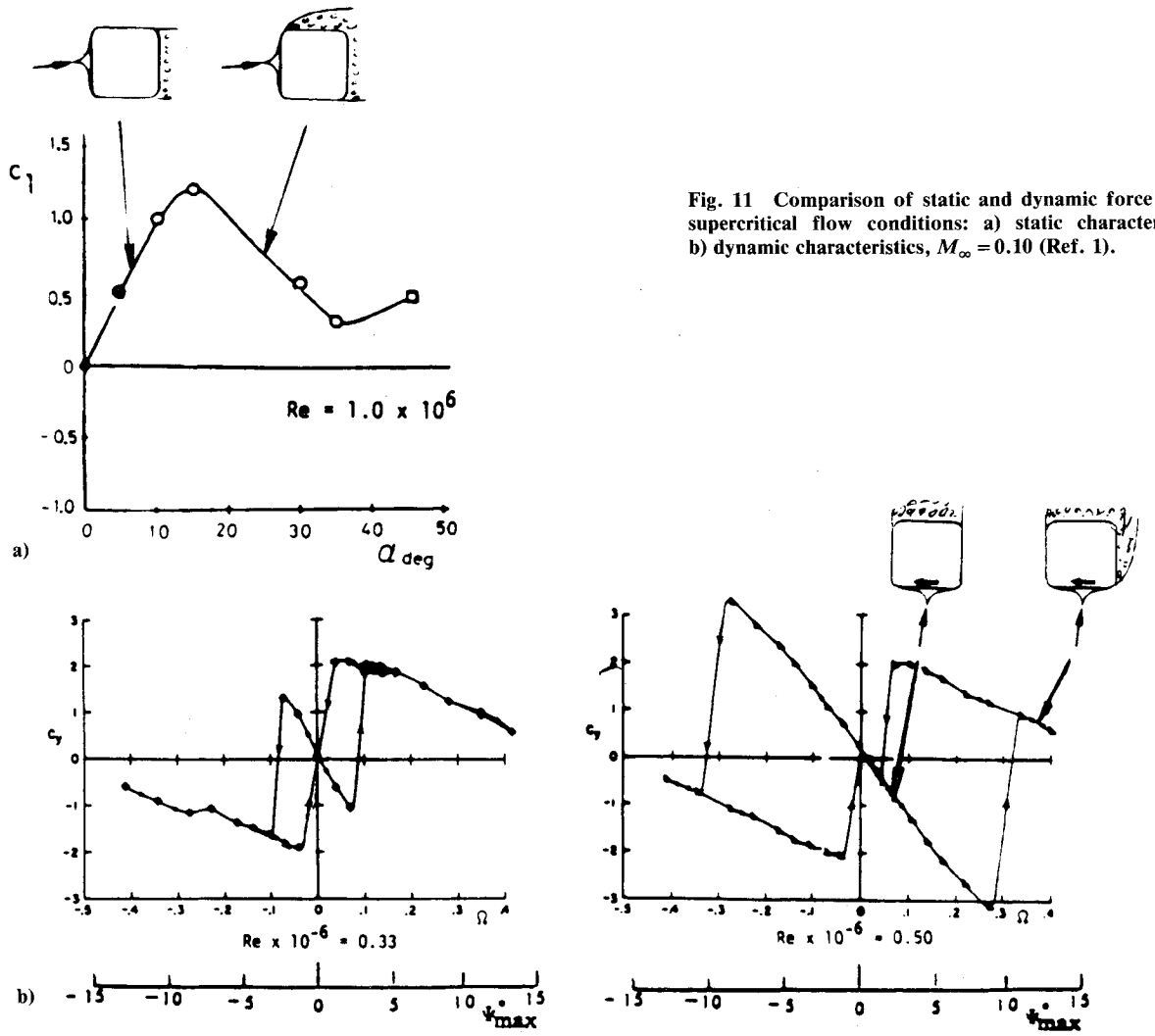

Fig. 11 Comparison of static and dynamic force characteristics at supercritical flow conditions: a) static characteristics (Ref. 18), b) dynamic characteristics, $M_\infty = 0.10$ (Ref. 1).

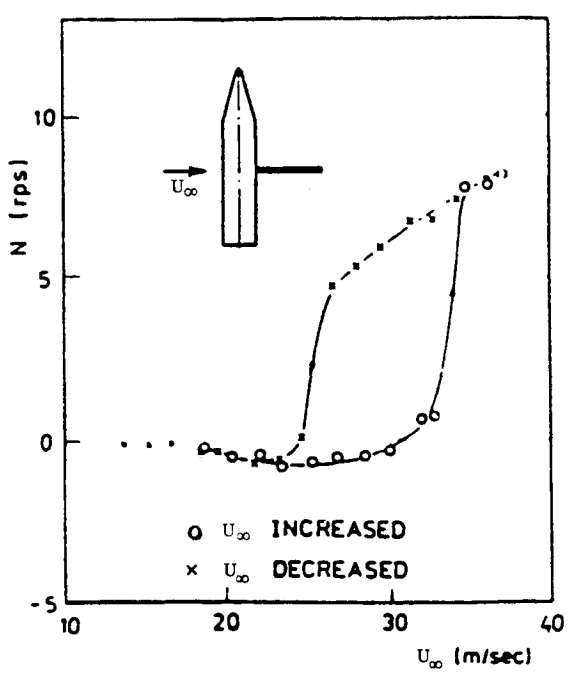

Fig. 12 Hysteresis effects on flat spin response of a cone cylinder.[19]

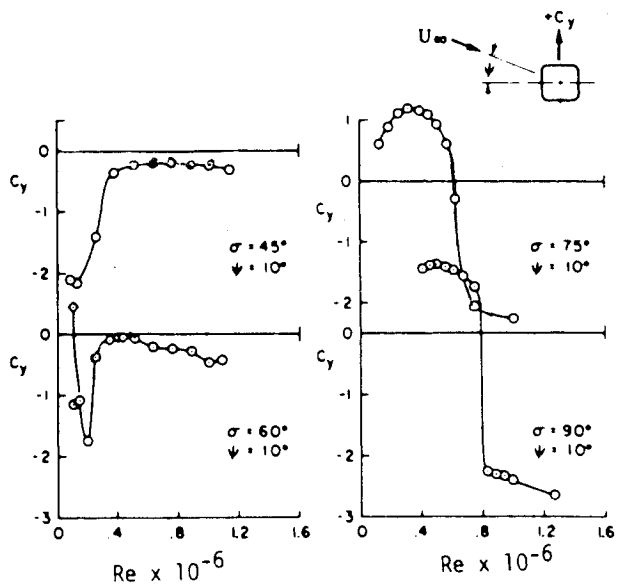

Fig. 13 Static side force characteristics for a square cross-sectional body.[1]

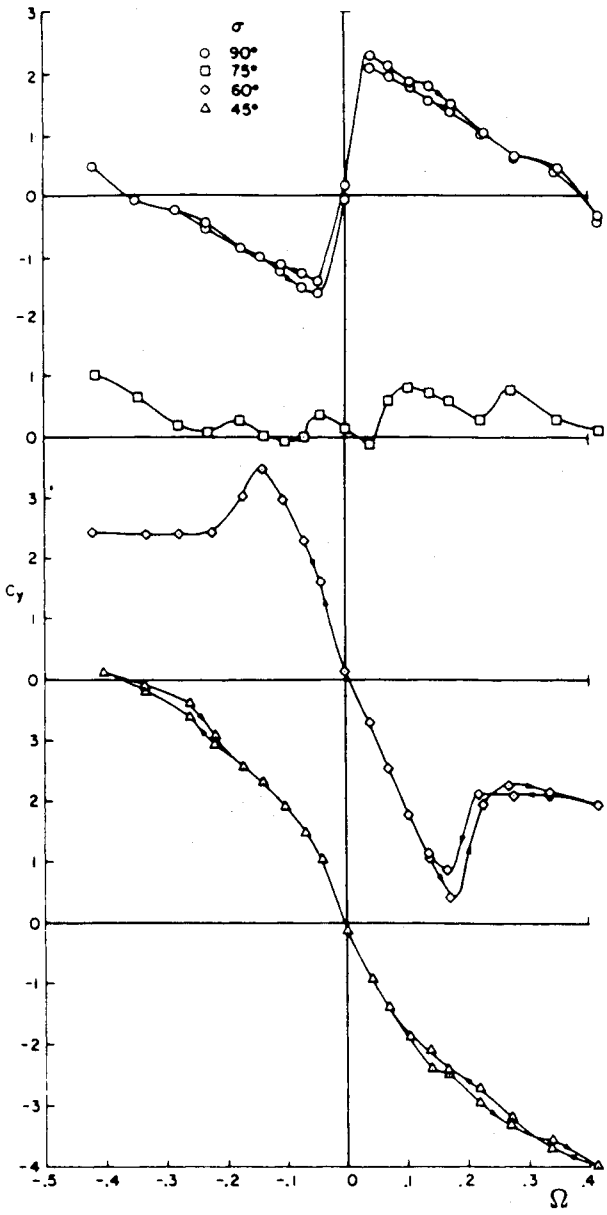

Fig. 14 Effect of coning angle σ at $M_\infty = 0.10$ and $Re = 0.15 \times 10^6$ (Ref. 1).

magnitude at the critical flow condition.[20,21] For the square cross-sectional body, the side force becomes of negligible magnitude at $\sigma = 45$ and 60 deg for supercritical Reynolds numbers, where the vortex shedding occurs from the base.

Comparing the static results for $\alpha = 90$ deg in Fig. 13 with the flat spin results in Fig. 2 for the same Mach number, $M = 0.25$, one finds them to be in basic agreement with regard to the critical Reynolds number, both indicating that supercritical attached-flow conditions are established at $Re = 0.75 \times 10^6$. For flow inclinations below $\sigma = 90$ deg, especially for the steady asymmetric vortex shedding occurring at $\sigma \leq 60$ deg, axial flow helps to establish attached-flow conditions already at $Re = 0.15 \times 10^6$ (Fig. 14). At $\sigma = 90$ deg, the Reynolds number would have to exceed $Re = 0.50 \times 10^6$ to accomplish this (cf. Figs. 2 and 14).

Conclusions

An analysis of experimental results for bodies of square cross section, describing coning motions at high angles of attack, has led to the following conclusions.

1) The unsteady wall boundary condition, the so-called moving wall effect, has a dominating influence on the forebody side force of the coning body.

2) The effects of moving wall velocity and Reynolds number combine to determine the highly nonlinear aerodynamics, including the extent of coning rate hysteresis effects at critical and low supercritical Reynolds numbers.

3) Decreasing the coning angle from the flat spin value $\sigma = 90$ to ≤ 60 deg promotes the establishment of supercritical attached-flow conditions, which as a result occur at much lower Reynolds numbers than in the flat spin case.

References

[1]Malcolm, G. N. and Clarkson, M. H., "Wind Tunnel Testing with a Rotary-Balance Apparatus to Simulate Aircraft Spin Motions," *Proceedings of the AIAA 9th Aerodynamic Testing Conference*, June 1976, pp. 143-146.

[2]Clarkson, M. H., Malcolm, G. N., and Chapman, G. T., "Experimental Post-Stall Rotary Aerodynamic Coefficients of Airplane-Like Configurations," *Journal of Aircraft*, Vol. 13, Aug. 1976, pp. 565-570.

[3]Malcolm, G. N., "Impact of High-Alpha Aerodynamics on Dynamic Stability Parameters of Aircraft and Missiles," AGARD LS-114, Lecture 2, March 1981.

[4]Ericsson, L. E., "Karman Vortex Shedding and the Effect of Body Motion," *AIAA Journal*, Vol. 18, Aug. 1980, pp. 935-944.

[5]Ericsson, L. E. and Reding, J. P., "Steady and Unsteady Vortex-Induced Asymmetric Loads on Slender Vehicles," *Journal of Spacecraft and Rockets*, Vol. 18, March-April 1981, pp. 97-109.

[6]Ericsson, L. E., "Maximum Crossflow Response of a Circular Cylinder, a Non-Resonant Flow Phenomenon," AIAA Paper 84-0508, Jan. 1984.

[7]Achenbach, E., "Influence of Surface Roughness on the Cross-Flow Around a Circular Cylinder," *Journal of Fluid Mechanics*, Vol. 46, Pt. 2, 1971, pp. 321-335.

[8]Zollars, G. J., Yechout, T. R., Daniel, D. C., and Lijewski, L. E., "Experimental Aerodynamics Characteristic of Missiles with Square Cross Sections," USAFA-TN-83-8, May 15, 1983.

[9]Ericsson, L. E. and Reding, J. P., "Dynamics of Forebody Flow Separation and Associated Vortices," *Journal of Aircraft*, Vol. 22, April 1985, pp. 329-335.

[10]Fiechter, M., "Uber Wirbelsysteme an schlanken Rotationskörpern und ihren Einfluss auf die aerodynamischen Beiwerte," Bericht 10/66, Deutsch-Französisches Forchungsinstitut, Sant Louis, France, Dec. 1966.

[11]Tarzanin, F. J. Jr., "Prediction of Control Loads Due to Blade Stall," *Journal of the American Helicopter Society*, Vol. 17, April 1972, pp. 33-46.

[12]Nakamura, Y. and Mizota, T., "Aerodynamic Characteristics and Flow Patterns of a Rectangular Block," *Reports of Research Institute for Applied Mechanics*, Kyushu University, Japan, Vol. XIX, No. 65, March 1972.

[13]Nakamura, Y. and Tomonari, Y., "Pressure Distributions on Rectangular Prisms at Small Incidence," *Transactions, Japan Society for Aeronautical and Space Science*, Vol. 21, No. 54, 1979, pp. 205-213.

[14]Ericsson, L. E. and Reding, J. P., "Analytic Prediction of Dynamic Stall Characteristics," AIAA Paper 72-682, June 1972.

[15]Ericsson, L. E. and Reding, J. P., "Dynamic Stall Analysis in Light of Recent Numerical and Experimental Results," *Journal of Aircraft*, Vol. 13, April 1976, pp. 248-255.

[16]Ericsson, L. E. and Reding, J. P., "Dynamic Stall at High Frequency and Large Amplitude," *Journal of Aircraft*, Vol. 17, March 1980, pp. 136-142.

[17]Parkinson, G. V., "Aeroelastic Galloping in One Degree of Freedom," *Proceedings of the Conference on Wind Effects on Buildings and Structures*, England, June 1963, Vol. II, HMSO, London, 1965, pp. 582-609.

[18]Polhamus, E. C., "Effect of Flow Incidence and Reynolds Number on Low-Speed Aerodynamic Characteristics of Several Non-circular Cylinders with Applications to Directional Stability and Spinning," NASA TR R-29, 1959.

[19]Kubota, H., Irai, I., and Matsuzaka, M., "Wind Tunnel Investigations for the Flat Spin of Slender Bodies at High Angles of Attack," AIAA Paper 82-0054, Aug. 1982.

[20]Ericsson, L. E. and Reding, J. P., "Review of Vortex-Induced Asymmetric Loads—Part I," *Zeitschrift für Flugwissenschaften und Weltraumforschung*, Vol. 5, Heft 3, 1981, pp. 162-174.

[21]Ericsson, L. E. and Reding, J. P., "Review of Vortex-Induced Asymmetric Loads—Part II," *Zeitschrift für Flugwissenschaften und Weltraumforschung*, Vol. 5, Heft 6, 1981, pp. 349-366.